Journal of Magnetic Resonance **151,** 124–128 (2001)
doi:10.1006/jmre.2001.2349, available online at http://www.idealibrary.com on IDEAL®

A Bridged Loop–Gap S-Band Surface Resonator for Topical EPR Spectroscopy

Sergey Petryakov, Michael Chzhan, Alexandre Samouilov, Guanglong He, Periannan Kuppusamy, and Jay L. Zweier

The EPR Center and Division of Cardiology, Department of Medicine, The Johns Hopkins University School of Medicine, 5501 Hopkins Bayview Circle, Baltimore, Maryland 21224

Received February 9, 2001; revised April 6, 2001

The design and structure of a bridged loop–gap surface resonator developed for topical EPR spectroscopy and imaging of the distribution and metabolism of spin labels in *in vivo* skin is reported. The resonator is a one-loop, one-gap bridged structure. A pivoting single loop-coupling coil was used to couple the microwave power to the loop–gap resonant structure. A symmetric coupling circuit was used to achieve better shielding and minimize radiation. The frequency of the resonator can be easily adjusted by trimming the area of the capacitive foil bridge, which overlaps the gap in the cylindrical loop. The working frequency set was 2.2 GHz and the unloaded Q was 720. The B_1 field of this resonator was measured and spatially mapped by three-dimensional EPR imaging. The resonator is well suited to topical measurements of large biological subjects and is readily applicable for *in vivo* measurements of free radicals in human skin.

Key Words: *in vivo* **EPR; loop–gap resonator; topical spectroscopy; EPR imaging; skin imaging; spin label.**

INTRODUCTION

EPR spectroscopy and imaging techniques have been applied to measure the concentration, kinetics, and spatial distribution of free radicals in biological tissues, *in vivo* living animals, and recently in humans (*1–3*). Nitroxide radicals have been widely used as a spin label to assess the distribution and redox state in biological systems. These labels provide useful information regarding a variety of cellular properties including redox state, oxygenation, and membrane structure (*2, 3*). Topical spectroscopy has been applied to perform localized measurements in large living systems. With topical measurements higher sensitivity of localized regions located close to the surface of the large lossy biological sample, such as the skin or underlying tissues, can be obtained. Topical spectroscopy facilitates the use of higher RF or microwave frequencies and enables higher resonator filling factors to be achieved for localized regions of interest. Because of these advantages, topical spectroscopy has been used for the first applications of EPR spectroscopy in humans (*1, 3*) and there has been particular interest in measurements and imaging of free radicals in human skin.

For topical EPR spectroscopy or imaging of a given sample structure *in vivo* or *ex vivo*, particular consideration must be given to the design and operating frequency of the resonator. The design must be optimized to achieve the highest sensitivity while providing reasonably uniform microwave penetration to the desired depth. For skin spectroscopy and imaging measurements, the limited thickness of the skin, ~2 mm, enables the use of frequencies as high as 2 to 4 GHz, so that a surface resonator structure can be used up to S-band in order to maximize EPR sensitivity.

With the great interest in measuring free radicals in biomedical systems, over the past decade a variety of lumped circuit devices have been developed for these applications, including loop–gap and reentrant resonators (*4–11*). The bridged loop–gap resonator design was originally developed for higher frequency applications at X-band (*12*) but recently this type of design has also been used for applications at S-band (*1, 4*). The use of an appropriate S-band surface resonator would be expected to provide higher sensitivity than possible with topical resonator designs described previously at 1 GHz or lower frequencies (*13–17*). However, when the working frequency is higher, the depth of RF penetration in biological tissues will be less. In human skin measurements, since the thickness of skin is generally about 2 mm, there is no need to work at frequencies below S-band. Based on these considerations, a working frequency in the S-band range has been chosen for human skin spectroscopy and imaging measurements (*1, 3*).

For topical EPR measurements of free radicals in *in vivo* human skin a high-sensitivity and high-stability S-band surface resonator was developed. The design and construction, as well as EPR and microwave properties of this bridged loop–gap surface resonator, are described.

SURFACE RESONATOR DESIGN

A surface resonator for topical EPR measurements of skin or other biological samples should have an optimized size and geometry so that microwave energy adequately penetrates out from the resonator into the applied surface of the sample. To satisfy the application requirements for topical EPR spectroscopy

1090-7807/01 $35.00

and imaging, the resonator B_1 magnetic field must extend beyond the end of the resonator to the depth of interest within the biological sample. The orientation of the B_1 field also must be perpendicular to the static magnetic field, B_0. With its loaded surface the resonator must work as one resonant system, with one resonant frequency. Specifically for application of EPR spectroscopy and imaging to humans, it is important for the resonator also to be compact, sturdy, durable, easy to couple, stable, and nonmicrophonic.

A resonator with axially oriented B_1 magnetic field was constructed using a cylindrical bridged loop–gap design with cylindrical shield to reduce microwave radiation. The topical sample is positioned in the plane of the opening, and thus, B_1 field penetrates the sample mostly perpendicular to its surface. Figures 1 and 2 show the mechanical layout of the one-loop, one-gap bridged surface resonator with pivoting loop-coupling mechanism. It contains a single inductive loop with a capacitive gap, a cylindrical shield with a Teflon body, and a single-loop coupling coil. The symmetric matching circuit consists of two twisted isolated conductors. The length of the matching circuit is approximately one-quarter of the wavelength and the impedance of the matching circuit is approximately 200 ohm.

The bridged loop–gap resonator was made using two quartz tubes. The outer diameter of the inner quartz tube was 8 mm, while the outer diameter of the outer quartz tube was 10 mm, with an inner diameter slightly greater than 8 mm. The silver foil of the resonator loop is attached to the outer surface of the inner tube while the silver layer of the bridge is attached on the outer wall of the outer tube as illustrated in Figs. 1 and 2. The thickness of the foil is 25 μm, the width of the foil, Z, is 22 mm, and the diameter of inductance loop, d, is 8 mm so that it is smaller than one-quarter of the wavelength to decrease radiation. Another small piece of silver foil was attached to the outer surface of the outer coaxial quartz tube to form the bridge as shown in Fig. 1. The width of the silver foil bridge, b, is 4 mm. The distance between the small foil bridge and the inner foil loop was

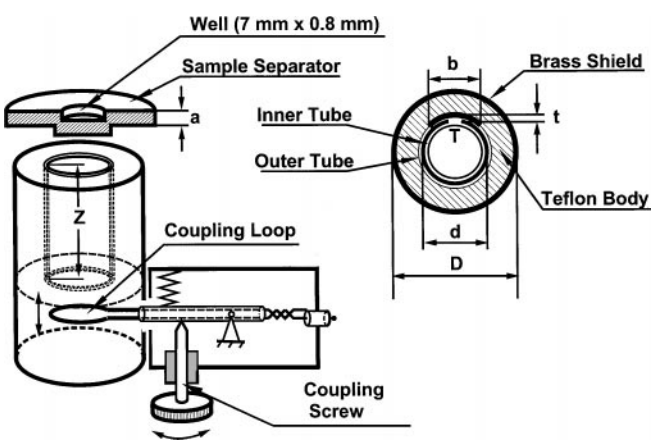

FIG. 1. Diagram of the mechanical layout of the S-band surface resonator. Values of the labeled dimensions of the resonator are defined in the text.

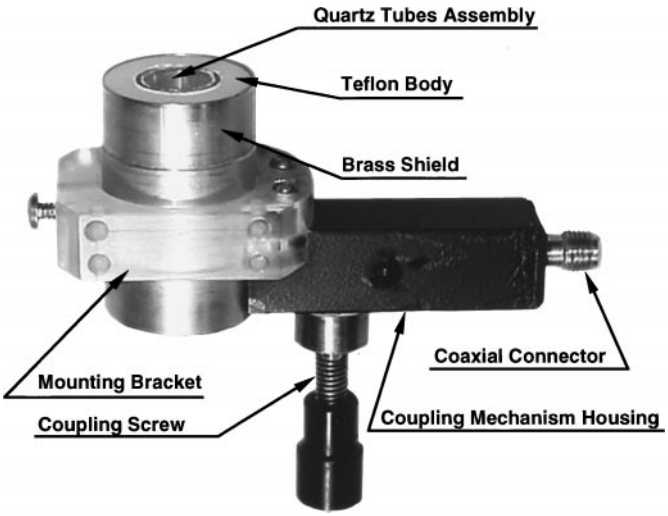

FIG. 2. Photograph of the S-band surface resonator.

determined by the thickness of the wall of the outer tube, t, which is 1 mm. The electrical shield was tightly attached to the outer surface of the Teflon holder as shown in Fig. 1. The diameter of the shield, D, is 21 mm. It is possible to adjust the resonant frequency, as much as 20%, by adjusting the width of the silver foil bridge on the outer tube as well as by rotation of the outer tube by a small angle thus changing the overlap of the bridge. The diameter of the coupling coil is the same as the inductance loop. An adjusting pivot mechanism was used as shown in Fig. 1 to change the distance of the coupling loop to the resonant loop. The length of the inductance tube, Z, was carefully chosen for optimization of the filling factor while maintaining sufficient Q when loaded, for operation of the AFC of the microwave bridge. A symmetric matching circuit with respect to ground was used as shown. A sample separator/sample holder disk was attached to the end of the resonator which served to protect the resonator from biological fluids and to fix the distance of the sample to assure proper microwave loading of the resonator (Fig. 1). This piece or similar ones was used to maintain a sample distance of $\sim$1.0 mm from the end of the resonator loop. For the phantom samples measured, this piece had a well of 0.8-mm depth and the disk thickness, a, was $\sim$1.8 mm.

MEASUREMENT OF RESONATOR MICROWAVE PROPERTIES

The microwave properties of the resonator including resonant frequency, Q, and B_1 were measured using a vector network analyzer, Agilent 8719 ES. The unloaded Q, Q_u, was determined as twice the measured Q value of the critically coupled resonator. The resonant frequency was 2.2 GHz and the unloaded Q_u was 720. With loading with water, normal saline, or large lossy biological tissues, as expected, the resonator Q drops substantially with a modest decrease in resonant frequency (Table 1). The

TABLE 1
Microwave Parameters of the Topical Resonator

f_o (MHz) unloaded	Q_u unloaded	f_o (MHz) water	Q_u water	f_o (MHz) saline	Q_u saline	f_o (MHz) skin	Q_u forearm	B_1^c (G/W$^{1/2}$) at surface
2212	720	2200	566	2200	458	2209	140	0.62

B_1 field was measured by the method of perturbing conducting spheres (*18*). Using a 2-mm-diameter brass conducing sphere, the B_1 field per square root of applied power was measured to be 0.62 G/(watt)$^{1/2}$ at the center position of the sample separator, 1 mm from the end of the resonator, (Fig. 1). We defined the B_0 direction in our spectrometer system as the Z direction. B_1 is along the Y direction. B_1 and B_0 are perpendicular to each other. The surface of the resonator is in the ZX plane and the orientation of the gap is in the ZY plane. As expected, the B_1 field decreases with distance perpendicular to the surface of the resonator, defined as along the Y-axis, or in-plane distance from the center of the resonator along the Z-axis or X-axis. EPR imaging was applied to fully define the relative B_1 field distribution in three-dimensional space as described below.

APPLICATION OF THE RESONATOR FOR EPR MEASUREMENTS

In order to test the sensitivity of the resonator and the feasibility of using it for *in vivo* EPR spectroscopy and imaging, experiments were performed on a topical phantom. A specially designed sample holder with a well in the middle was used (*1*). The well has a 7-mm diameter and 0.8-mm depth. A total of 30 μl of 0.5 mM ^{15}N-PDT (perdeuterated tempone) saline solution was pipetted into the well and the well was sealed with a self-stick tape. Then the holder with the nitroxide solution was placed onto the top of the surface resonator. EPR spectroscopy measurements were performed on a laboratory-built S-band spectrometer with spectroscopy and imaging capability (*1*). The microwave bridge components included an oscillator (CC-24, Engelmann Microwave, Whippany, NJ), isolator (CT-3240-OT, UTE, Microwave, Inc., Asbury Park, NJ), circulator (CT-3242-OT UTE Microwave, Inc), directional coupler (CL-2040-20, EMCO, Broomfield, CO), attenuator (AC9003-69-31, Weinschel Corp, Lexington, MA), and schottky diode detector (DSL204P Herotek, Inc, San Jose, CA) (*1*). The EPR spectroscopy parameters were as follows: frequency, 2.2 GHz; microwave power, 50 mW; modulation amplitude, 0.5 G; scan width for the whole spectrum, 60 G; scan time, 15 s; time constant, 80 ms.

Figure 3A shows the spectrum from 30 μl of 0.5 mM ^{15}N-PDT (perdeuterated tempone) saline solution that was pipetted into the well in the sample separator shown in Fig. 1. The insert in the figure shows the baseline with a 100-fold higher gain and we calculate that the signal-to-noise ratio is about 1000 to 1.

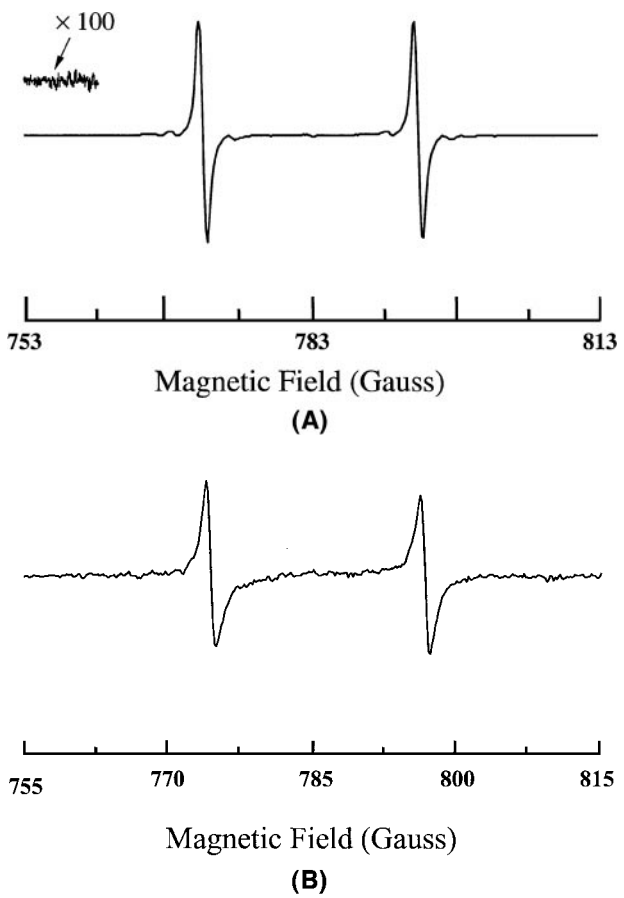

FIG. 3. EPR spectra obtained using the surface resonator. A, Spectrum obtained from a sample phantom. The phantom consists of a specially designed sample holder with a well in the middle of 7-mm diameter and 0.8-mm thickness. A total of 30 μl 0.5 mM ^{15}N-PDT saline solution was pipetted into the well and the well was sealed with self-stick tape. The holder with the nitroxide solution was placed onto the top of the surface resonator. The inset shows the tracing at 100-fold increased gain. B, *In vivo* EPR measurement of nitroxide radicals in the forearm skin of a human volunteer performed using the surface resonator. A total of 3 μl of 10 mM ^{15}N-PDT water solution was applied to the surface of human skin within a circular spot of 6-mm diameter. Spectra were recorded after 60 min to allow penetration and diffusion of the nitroxide into the skin (*1*). Both spectra (A and B) were recorded at a frequency of 2.2 GHz with 50 mW of microwave power, modulation amplitude 0.5 G, scan time 15 s, and time constant 80 ms.

With this sensitivity, *in vivo* and *in vitro* EPR spectroscopy and imaging applications can be performed including measurements and spatial mapping of nitroxide radicals in human skin (*1*). As shown in Fig. 3B, good quality *in vivo* EPR spectra could also be rapidly obtained from small amounts ($\approx 10^{-8}$ mol) of nitroxide labels applied to the forearm skin of human volunteers.

Of note with regard to large samples, it is important for this S-band resonator, as well as prior topical EPR surface resonators (*13–17*), that the sample with paramagnetic material not extend significantly beyond the diameter of the resonator into the path of return flux. If the sample extends beyond the diameter of the loop into the path of the return flux the orientation of the B_1 field varies and distortion of the observed EPR signal will occur.

MAPPING OF THE RESONATOR B_1 FIELD USING EPR IMAGING

Three-dimensional spatial EPR imaging was performed to determine the relative B_1 distribution along the X-, Y-, and Z-axes as a function of the distance from the center of the resonator surface. A cylindrical rexolyte tube with inner diameter of 7.9 mm and height of 16.7 mm was filled with 0.5 mM aqueous TAM solution (Nycomed) that has an ideal sharp single line EPR spectrum as described previously (*19*). The phantom was positioned 1 mm away from the surface of the resonator by a sample separator/sample holder disk. The center of the bottom of the cylinder was defined as the origin. The magnet system, gradient setup, and imaging instrumentation used were as previously described (*20*). Image reconstruction and deconvolution were performed as previously described (*19*). A set of large modulation coils (128-mm diameter) was used, attached to the inner walls of the gradients with a distance of 64 mm, and this provides $>90\%$ modulation field homogeneity over the central 10 mm diameter spherical space where the resonator surface and active volume is centered. The imaging parameters were chosen as follows: magnetic field gradient 8 G/cm, spatial window 13 mm, modulation amplitude 0.2 G, modulation frequency 100 kHz, scan width 10.4 G, scan time 5.24 s, time constant 40 ms, number of projections 576. Figure 4 shows three slices of the 3D image depicting the correspondent image intensity profiles from the 3D image. All three slices intersect the origin. Using the B_1 per square root power value of 0.62 $G/\sqrt{W}$ at 1 mm off the surface of the resonator, determined above, the image intensity profiles were calibrated to provide the B_1 per square root power distribution as shown in Fig. 4. From the images and the B_1 profiles

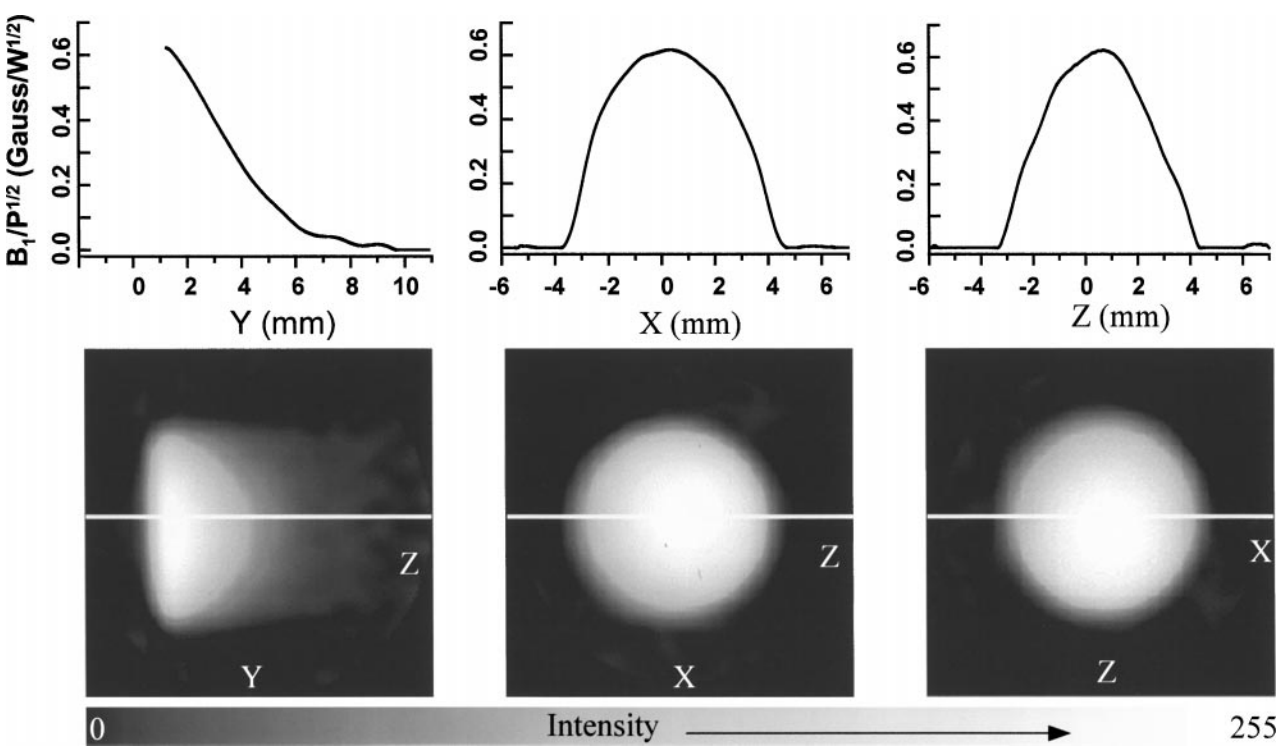

FIG. 4. Measurement and imaging of the B_1 profile of the surface resonator. Three-dimensional spatial EPR imaging was performed to determine the relative B_1 distribution along the X-, Y-, and Z-axes as a function of the distance from the center of the resonator surface. A cylindrical rexolyte tube with inner diameter of 7.9 mm and height of 16.7 mm was filled with 0.5 mM TAM radical label. The imaging parameters were as follows: magnetic field gradient 8 G/cm, spatial window 13 mm, modulation amplitude 0.2 G, scan time 5.24 s, time constant 40 ms, number of projections 576. Three slices of the 3D image are shown depicting the image intensity profiles normal to the X-, Y-, or Z-axes. Using the B_1 per square root power value of 0.62 $G/\sqrt{W}$ measured at 1 mm off the surface at the center of the resonator, the image intensity profiles were calibrated to provide the B_1 per square root power distribution.

obtained, it was observed that along the axis perpendicular to the plane of the resonator surface, the Y-axis of the image, the resonator can detect the EPR signal up to a ~6-mm distance. Up to a distance of 2 mm along the Y-axis, the B_1 field remained within ~70% of its maximum. Over the XZ plane of the image going through the origin, the resonator can detect the EPR signal within a diameter of ~7 mm and the B_1 field remained within 70% of its maximum over a diameter of ~4.5 mm.

CONCLUSIONS

We describe an S-band bridged loop–gap resonator design developed to enable the topical EPR measurements in the skin of living animals or humans. The resonator operates at 2.2 GHz with an unloaded Q of 720 and the Q remains relatively high with topical use with a value of ≈140 in the presence of large lossy samples applied to its surface. It is inductively coupled and the pivoting coupling loop provides the requisite range of coupling. This resonator enables detection of amounts of nitroxide spin label of 15 nmol with a signal-to-noise ratio of 1000 in a 15-s acquisition. This resonator has been successfully used to measure the kinetics of nitroxide metabolism and image the spatial distribution of nitroxides in the skin of normal human volunteers [1]. The resonator design is durable and suitable for a range of topical applications in *in vivo* animals and in humans.

ACKNOWLEDGMENTS

We thank Nycomed Innovation for providing the TAM label. This work was supported by NIH Grants RR12190 and GM58582.

REFERENCES

1. G. He, A. Samouilov, P. Kuppusamy, and J. L. Zweier, *In vivo* EPR imaging of the distribution and metabolism of nitroxide radicals in human skin, *J. Magn. Reson.* **148,** 155–164 (2001).
2. J. L. Zweier and P. Kuppusamy, Electron paramagnetic resonance measurements of free radicals in the intact beating heart: A technique for detection and characterization of free radicals in whole biological tissues, *Proc. Natl. Acad. Sci. USA* **85,** 5703–5707 (1988).
3. J. Fuchs, N. K. Groth, T. E. Herrling, and G. Zimmer, Electron paramagnetic resonance studies on nitroxide radical 2,2,5,5-tetramethyl-4-pipen'din-oxyI (TEMPO) redox reactions in human skin, *Free Rad. Biol. Med.* **22,** 967–976 (1997).
4. M. Willer, J. Forrer, J. Keller, S. V. Doorslaer, A. Schweiger, R. Schuhmann, and T. Weiland, S-band (2–4 GHz) pulse electron paramagnetic resonance spectrometer: Construction, probe head design, and performance, *Rev. Sci. Instrum.* **71,** 2807 (2000).
5. W. Froncisz and J. S. Hyde, The loop–gap resonator: A new microwave lumped circuit ESR sample structure, *J. Magn. Reson.* **47,** 515–521 (1982).
6. J. S. Hyde, and W. Froncisz, Loop–gap resonators, *Electron Spin Reson.* 10A, 175–184 (1986).
7. R. Diodato, M. Alecci, J. A. Brivati, V. Varoli, and A. Sotgiu, An optimization of axial RF field distribution in low-frequency EPR loop–gap resonators, *Phys. Med. Biol.* **44**(5), N69–N75 (1999).
8. G. A. Rinard, R. W. Quine, B. T. Ghim, S. S. Eaton, and G. R. Eaton, Easily tunable crossed-loop (bimodal) EPR resonator, *J. Magn. Reson. A* **122,** 50–57 (1996).
9. M. Chzhan, M. Shteynbuk, P. Kuppusamy, and J. L. Zweier, An optimized L-band ceramic resonator for EPR imaging of biological samples, *J. Magn. Reson. A* **105,** 49–53 (1993).
10. M. Chzhan, P. Kuppusamy, and J. L. Zweier, Development of an electronically tunable L-band resonator for EPR spectroscopy and imaging of biological samples, *J. Magn. Reson. B* **108,** 67–72 (1995).
11. M. Chzhan, P. Kuppusamy, A. Samouilov, G. L. He, and J. L. Zweier, A tunable reentrant resonator with transverse orientation of electric field for *in vivo* EPR spectroscopy, *J. Magn. Reson.* **137**(2), 373–378 (1999).
12. S. Pfenninger, J. Forrer, A. Schweiger, and T. Weiland, Bridged loop gap resonator, a resonant structure for pulsed electron-spin-resonance transparent to high-frequency radiation, *Rev. Sci. Instrum.* **59,** 752–760 (1988).
13. L. J. Berliner and H. Fujii, Magnetic resonance imaging of biological specimens by electron paramagnatic resonance of nitroxide spin lables, *Science* **227,** 517–519 (1985).
14. T. Walczak and H. M. Swartz, A GHz *in vivo* ESR spectrometer with a surface probe. *Phys. Med.* **5,** 195–202 (1989).
15. H. Hirata, T. Walczak, and H. M. Swartz, Electronically tunable surface-coil-type resonator for L-band EPR spectroscopy, *J. Magn. Reson.* **142,** 159–167 (2000).
16. P. Kuppusamy, M. Afeworki, R. A. Shankar, D. Coffin, M. C. Krishna, S. M. Hahn, J. B. Mitchell, and J. L. Zweier, *In vivo* electron paramagnatic resonance imaging of tumor heterogeneity and in a murine model, *Cancer Res.* **58,** 1562–1568 (1998).
17. P. Kuppusamy, P. Wang, R. A. Shankar, L. Ma, C. E. Trimble, C. J. C. Hsia, and J. L. Zweier, In vivo topical EPR spectroscopy and imaging of nitroxide free radicals and polynitroxyl–albumin, *Magn. Reson. Med.* **40,** 806–811 (1998).
18. J. H. Freed, D. S. Leniart, and J. S. Hyde, Theory of saturation and double resonance effects in ESR spectra. III. Rf coherence and line shapes, *J. Chem. Phys.* **47,** 2762–2773 (1967).
19. P. Kuppusamy, P. Wang, M. Chzhan, and J. L. Zweier, High resolution electron paramagnatic resonance imaging of biological samples with a single line paramagnatic label, *Magn. Reson. Med.* **37,** 479–483 (1997).
20. G. He, R. A. Shankar, M. Chzhan, A. Samouilov, P. Kuppusamy, and J. L. Zweier, Noninvasive measurement of anatomic structure and intraluminal oxygenation in the gastrointestinal tract of living mice with spatial and spectral EPR imaging, *Proc. Natl. Acad. Sci. USA* **96,** 4586–4591 (1999).